Blending drifters and altimetric data to estimate surface currents: Application in the Levantine Mediterranean and objective validation with different data types

Georges Baaklini [a,b], Leila Issa [c], Milad Fakhri [b], Julien Brajard [a,d], Gina Fifani [a,b], Milena Menna [f], Isabelle Taupier-Letage [e], Anthony Bosse [e], Laurent Mortier [a]

[a] Sorbonne University, UPMC Univ Paris 06 CNRS-IRD-MNHN, LOCEAN Laboratory, 4 place Jussieu, 75005 Paris, France
[b] National Centre for Marine Sciences-CNRSL, P.O. Box 189, Jounieh, Lebanon
[c] Department of Computer Science and Mathematics, Lebanese American University, Beirut, Lebanon
[d] Nansen Environmental and Remote Sensing Center, Bergen, Norway
[e] Aix Marseille Univ., Universite de Toulon, CNRS, IRD, MIO UM 110, 13288, Marseille, France
[f] National Institute of Oceanography and Applied Geophysics (OGS) Borgo Grotta Gigante, 42/c 34010 Sgonico (Trieste), Italy

ARTICLE INFO

Keywords:
Altimetry
Lagrangian data
Data assimilation
Drifters
Surface velocity field
Levantine Mediterranean

ABSTRACT

An improved estimation of the surface currents in the Levantine Basin of the Mediterranean sea is crucial for a wide range of applications, including pollutants transport and nutrients distribution. This estimation remains challenging due to the scarcity or shortcomings of various data types used for this purpose. In this paper, we present an objective validation of a variational assimilation algorithm that blends geostrophic velocities derived from altimetry, wind-induced velocities, and drifter positions, to continuously obtain velocity corrections. The assessment of the validation impact was based on available independent in-situ data (current meters, gliders, and independent drifters) and satellite ocean color images. In all cases, the improvement was shown either qualitatively (position of the eddies) or quantitatively.

1. Introduction

The surface circulation in the southern part of the Mediterranean sea along the North African coasts is characterized by the presence of unstable currents that generate mesoscale eddies (see, e.g, Robinson et al. (1992), Millot and Taupier-Letage (2005), Amitai et al. (2010) and Schroeder et al. (2012)). These eddies have diameters of 10–100 km and lifetimes that can span several months to years (see, e.g, Puillat et al. (2002), Hamad et al. (2006), Mkhinini et al. (2014) and Pessini et al. (2020)). Mesoscale activity in the Eastern Mediterranean is intense with high eddy kinetic energy (more than 700 cm^2/s^2) recorded historically (see, e.g, Robinson et al. (1992), Pujol and Larnicol (2005) and Gerin et al. (2009)). Mesoscale eddies can interact, split or merge, and induce smaller-scale structures (shear-eddies and filaments). Thus tracking them is a real challenge (see, e.g, Taupier-Letage et al. (2003), d'Ovidio et al. (2004), Laxenaire et al. (2018) and Le Vu et al. (2018)). All these structures can transport coastal waters, trap and advect on large distances tracer anomalies. Such activity has a continuous and direct impact on biogeochemical water properties, especially in the redistribution of nutrient-rich coastal waters into the oligotrophic open sea (see, e.g, Taupier-Letage et al. (2003), Lehahn et al. (2007), Levy and Martin (2013) and Escudier et al. (2016)) and the dispersion of pollutants. An accurate and continuous estimation of surface circulation is therefore needed, but remains challenging.

Even though more and more data, in particular, operational products from the Copernicus Marine Service (marine.copernicus.eu) are available for estimating surface currents at (sub)mesoscale, each on their own, have their limitations. A powerful tool that is widely used to describe the mesoscale features of surface circulation is the state of the art satellite altimetry. Multi-mission gridded altimeter products originated from Copernicus Marine Service have the advantage of providing uninterrupted and continuous global surface velocities (Caballero et al., 2013). Nevertheless, there are still uncertainties associated with these products: relative low spatial resolution of current radar altimetry; satellite information is degraded near the coastal areas within 20–50 km from land (Cipollini et al., 2010); incorrect removal of high-frequency atmospheric effects that exist at the sea surface (Caballero et al., 2013), Mean Dynamic Topography (MDT) is not always precisely known in the basin. Moreover, the problem accentuates in the

Mediterranean Sea where a precise knowledge of MDT is still an issue, due to the presence of narrow straits and a high number of islands, and the small Rossby radius of deformation of around 10 km that makes the altimeter-resolution insufficient to capture the small details (Rio et al., 2014). Due to the coarse resolution in both space and time of the altimeters, and to the fact that mesoscale structures move continuously, eddies can be missed, artificially created, smoothed or misplaced (Mkhinini et al., 2014; Ioannou et al., 2017). Characterizing eddies using altimetry can lead to an underestimation of the eddies' density, especially the small ones. These eddies may be not captured by altimetry or tend to be aliased into larger structures compared to the true eddies (Amores et al., 2018).

In-situ observations are used as a tool to complement and/or validate altimetry (Le Traon and Hernandez, 1992). Drifters have the advantage of being autonomous and relatively inexpensive. They are in-situ Lagrangian tools following the ocean current once they are released and adequately equipped with a drogue (Poulain et al., 2012). Characterized by positive buoyancy, this restrains them along with the two-dimensional flow at the surface or near-surface of the ocean. Even though they help in providing a precise description of the surface circulation, their spatio-temporal distribution is not continuous, because they are typically short-lived and their spatial distribution is intrinsically uneven.

When large data sets are available, combining altimetric and drifter data can be done using statistical approaches (see, e.g, Niiler (2003), Uchida and Imawaki (2003), Poulain et al. (2009), Maximenko et al. (2009), Poulain et al. (2012), Menna et al. (2012) and Stanichny et al. (2016)). Alternatively, data can be assimilated in a variational approach in which corrections of the velocity are obtained by minimizing an objective function measuring the difference between observations and their corresponding model variables. Variational methods that take into account the temporal variation within the optimization are called 4D-Var (Kamachi and O'Brien, 1995; Mead, 2005; Nodet, 2006; Carrier et al., 2014; Muscarella et al., 2015). A more detailed review of various assimilation methodologies can be found in Issa et al. (2016).

From the application point of view, merging altimetry and in-situ data for a better estimation of the sea surface circulation has previously had several successful applications: for example in the Gulf of Mexico (Carrier et al., 2014; Muscarella et al., 2015; Berta et al., 2015), the Black Sea (Kubryakov and Stanichny, 2011; Stanichny et al., 2016), the North Pacific (Uchida and Imawaki, 2003), and the Mediterranean Sea (Taillandier et al., 2006; Menna et al., 2012; Issa et al., 2016), each of them using different methodologies for merging.

Validating these merged data sets using in-situ current meter data was done in Taillandier et al. (2006), where the comparison focused on the net transport time series representing the total volume flux over a selected area. Referring to long-term current meter measurements available across the Corsica Channel, the assimilation showed a 10% increase of the estimated net transport leading to instantaneous transport values that are closer to those observed by the current meter.

The variational assimilation algorithm used by Issa et al. (2016) proved its efficiency in the Eastern Levantine Mediterranean region, specifically along the Lebanese coast and in the region between Lebanon and Cyprus. Sensitivity analyses showed that the velocity estimation can be improved significantly even with only a small number of drifters. The algorithm that was developed relies on continuously correcting the altimetry-derived velocity by matching the observed drifters positions with those predicted by an advection model, taking into account the wind effect and imposing a divergence-free condition on the correction. The algorithm needed very few computational resources and converged quickly.

The contribution of the current work is two-fold: (i) a further extension of the application of the previous algorithm by Issa et al. (2016) in the Levantine Mediterranean and (ii) an objective validation of the algorithm, using reliable tools/data independent of the algorithm itself. In particular, we use four different types of independent data: first, a current meter moored off Libya is used to validate the algorithm results in terms of velocity intensity and direction. Second, a glider-derived near-surface absolute geostrophic velocity perpendicular to its trajectory is compared with the projected velocities obtained after assimilation. Third, we reproduce the path of a non-assimilated drifter by the simulation of its position using velocities obtained by the assimilation of two other drifters. Finally, we compare streamlines of the corrected velocity field with the shape of an eddy obtained by an ocean color satellite image. This offers a qualitative but useful comparison. Except for products from Copernicus operational forecast models or reanalysis, we believe that no other surface current data are available in the Levantine region for such a comparison.

The paper is structured as follows: we introduce the data used in the assimilation and validation in Section 2. In Section 3, we provide a brief recap of the algorithm used for the assimilation, as well as the sensitivity test done to optimally choose the parameters. In Section 4, we present the metrics used for validation. Finally, in Section 5, we show the results of the assimilation experiments, as compared with in-situ current meter data, ocean color satellite images, gliders. We also show the results of the independent drifters experiment.

2. Data

The study focuses on the Eastern part of the Mediterranean, that is less investigated than its western counterpart, more specifically on the Levantine basin. The data used for this study are listed in Sections 2.1–2.7:

2.1. Drifters data

The EGYPT/EGITTO program (Eddies and Gyres Paths Tracking, Taupier-Letage et al. (2007)) focused on the Eastern Mediterranean southern part spanning the period 2005–2007. It provided an extensive deployment of satellite-tracked drifters which helps in characterizing mesoscale and sub-mesoscale structures. (see the ~2-years trajectories animation on southeastern Mediterranean surface drifter database: nettuno.ogs.trieste.it/doga/sire/egitto/database_egitto/movies/sep05-oct07.avi). These drifters were tracked by the global Argos System. Their time series were interpolated at 0.5 h (Poulain et al., 2013). Data were then low-pass filtered using a Hamming filter with a cut-off period at 36 h to eliminate high-frequency current components (tidal and inertial currents).

In addition to those, we used drifters from the Surface Circulation in the Northeastern Mediterranean (NEMED) project from 2009 to 2010. NEMED is an observational program releasing drifters between Cyprus and the Middle East. Drifters time series were interpolated at 6 h. From this large drifters data set (97 drifters from EGYPT/EGITTO and 31 drifters from NEMED) (Menna et al., 2018), we selected drifters depending on each validation experiment. All drifters used in the assimilation are equipped with a positioned drogue located at 15 m depth, which reduces the wind forcing impact.

2.2. Altimetry data

Geostrophic surface velocity fields are processed by the DUACS (Data Unification and Altimeter Combination System) multi-mission altimeter data processing system and distributed by E.U. Copernicus Marine Service Information (CMEMS). The SLA computation provides the Absolute Dynamic Topography (ADT) and geostrophic currents. The gridded products are estimated by an optimal interpolation that merges measurements from several altimeter missions: HY-2 A, Jason-2, Jason-1, T/P, ENVISAT, GFO, ERS1/2. The interpolation provides a consistent and homogeneous database. Data were daily mapped at a resolution of 1/8°.

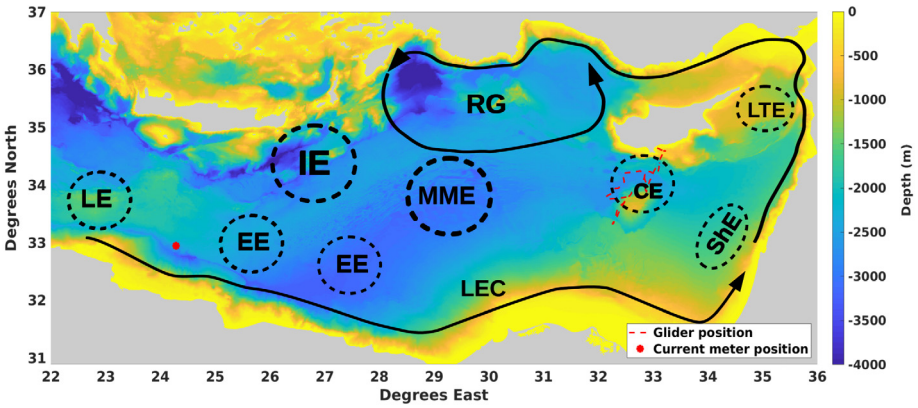


Fig. 1. A schematic representation of the main current structures based on the observations of Gerin et al. (2009) and Menna et al. (2012) in the Levantine basin (RG: Rhodes gyre, IE: Ierapetra eddy, LE: Libyan eddies, EE: Egyptian eddies, LEC: Libyo-Egyptian current, MME: Mersa-Matruh eddies (also known as Herodotus trough eddies), CE: Cyprus eddies, ShE: Shikmona eddies, LTE: Lattakia eddy). The location of the in-situ data used for validation is compared to these structures. The red star represents the mooring C_3 location off the Libyo-Egyptian coasts, during the EGYPT/EGITTO program, supporting the 60m-deep current meter used for the validation. The red dashed line south of Cyprus represents the glider trajectory. All is overlayed on a bathymetry map.

2.3. Wind data

Six-hourly wind data were obtained from ECMWF ERA-Interim products (Dee et al., 2011) at 10 m above the surface. Data was re-sampled on a half an hour time step. The product spatial resolution is approximately 0.7 degrees. Wind velocities were interpolated at a resolution of 1/8° at the same grid point as the AVISO background data although the actual resolution is much coarser.

2.4. Current meter

The first comparison focused on the area of the Libyo-Egyptian coast, where the anticyclonic eddies generated by the Libyo-Egyptian Current move offshore (Hamad et al., 2006). Between April 2006 and April 2007, 7 moorings each equipped with current meters were deployed off Libya during the EGYPT/EGITTO program (Taupier-Letage et al., 2007) to provide information on the circulation of the water masses. However, since only sub-surface moorings could be used because of safety issues, the surface layer of Atlantic Water was sampled at 60–100 m deep, and used to compare with the drifter (~15 m deep).

We selected the current meter that met the following criteria: a long record (since some moorings have been cut accidentally), fixed at ~60–100 m deep, and located on a mooring with a contemporary drifter passage. The shallowest current meter of the C_3 mooring (see Fig. 1) was the only one to meet all the criteria, as the mooring C3 was located near the passage path of the 1st selected drifter (Argos number: 57306) and providing data at less than 100 m depth.

2.5. Mediterranean Forecasting system (MFS)

The Mediterranean Forecasting System is a coupled hydrodynamic (from NEMO v3.6) and wave (provided by WaveWatch-III) model with data assimilation components implemented over the Mediterranean Basin. In-situ vertical profiles of temperature and salinity (from XBT, CTD, Argo floats) are assimilated with satellite Sea Level Anomaly along-track data (from Jason1&2, Cryosat, Envisat, Altika). The product quality assessment is done by comparing with quasi-independent satellite and in-situ observations. The model spatial resolution is 1/16°, and the product is computed on 72 unevenly-spaced vertical levels. The depths levels are unevenly spaced and the thickness varies from 3 m at the surface to 300 m at the bottom. The first level depth is at 1.5 m while the deepest one is at 5000 m (Tonani et al., 2008). The model outputs were used to evaluate the comparability between the current vector velocity fields at the current meter and the drifters depth as detailed in Section 4.1.

2.6. Gliders

Gliders are a type of robotic underwater vehicle that perform saw-tooth trajectories (Testor et al., 2019). The movement of the internal weights allows the glider to change its buoyancy. Thus, it dives or climbs in the water column. Moreover, the lift generated by the wings moving through the water converts vertical force into forwarding motion. In the context of the "Eye of the Levantine" experiment, gliders were deployed south of Cyprus in November and December 2010. Targeting the Cyprus warm core eddy, the transects followed a butterfly pattern near the Eratosthenes Seamount, extending to a maximum depth of 1000 m, collecting seawater characteristics such as temperature and salinity (Hayes et al., 2011). The water density sections and the depth-averaged current data derived from these glider positions are used to estimate profiles of absolute geostrophic velocity perpendicular to their trajectories (Eriksen et al., 2001). During the campaign, six gliders were deployed off Limassol towards the Cyprus eddy. From these gliders, we used the geostrophic velocities from the named "TRIESTE-1" glider. It was a coastal glider that dived at 200 m depth maximum and was circulating close to a drifter (Argos number: 92060). The obtained velocities used for the comparison corresponded to the near-surface absolute geostrophic velocities perpendicular to the glider track and averaged in the upper 20 m. The glider sampled the upper 200 m, and geostrophic shear was integrated to the surface from a low-pass filtered density section, where variability smaller than 15 km corresponding to unbalanced isopycnal displacement was removed by a moving average. This approach was applied in numerous studies in the past (see e.g. Bosse and Fer (2019)).

2.7. Ocean color

Eddies are oceanic structures with high vorticity able to modify the seawater physical distribution properties, thus affecting the distribution of marine phytoplankton communities (McGillicuddy Jr, 2016). Previous high-resolution chlorophyll images have shown that even small swirling and filamentary patterns of chlorophyll could be determined from satellite imagery. Therefore high resolution ocean color images could be an efficient tool for mesoscale features monitoring such as eddies. Their shape and location could be detected from chlorophyll-a concentration images, leading to a better understanding of these physical processes (Sarangi, 2012). These chlorophyll-a images detected the shape of an eddy trapping a contemporary drifter (Argos number: 57307). MODIS-Aqua chlorophyll level-2 data, at 1 km spatial resolution, corresponding to the days of assimilation for comparison were acquired from GSFC-NASA.

3. Assimilation algorithm

The correction is based on a variational assimilation method described in Issa et al. (2016). Observations of drifter's positions are available every Δt. We denote the background surface velocity field by

$$\mathbf{u}_m^b = \mathbf{u}^b(m\Delta t),\ m = 1, 2, \ldots, M, \tag{1}$$

where this field is two dimensional $\mathbf{u}_m^b = (u_m^b, v_m^b)$, and where m is the integer time index. This field is corrected by matching observed drifter's positions with those predicted by an advection model.

The background velocity field ($\mathbf{u}_m^{\mathrm{b}}$) used is the sum of a geostrophic component provided by altimetry ($\mathbf{u}_m^{\mathrm{geos}}$) and an ageostrophic component accounting for the effect induced by the wind ($\mathbf{u}_m^{\mathrm{wind}}$)

$$\mathbf{u}_m^b = \mathbf{u}_m^{\mathrm{geos}} + \mathbf{u}_m^{\mathrm{wind}}. \tag{2}$$

This wind-induced velocity is computed by the equation of Poulain et al. (2009) (for drifters that are attached with a drogue).

$$\mathbf{U}_m^{wind} = 0.007 \exp(-27°\, i) \times \mathbf{U}_m^{10} \tag{3}$$

where $\mathbf{U}_m^{wind} = u_m^{\mathrm{wind}} + i v_m^{\mathrm{wind}}$ is the drifter velocity due to the wind effect, and $\mathbf{U}_m^{10} = u_m^{10} + i v_m^{10}$ represents the wind velocity at 10 m above the surface. Both are expressed as complex numbers. The wind speed above the sea surface varies considerably at a very short time scale. Thus the wind-induced velocity field contribution to the total velocity depends on the varying weathering conditions.

An incremental approach (Talagrand and Courtier, 1987) is used so that the minimization is done for the incremental corrections $\boldsymbol{\delta}\mathbf{u}$ invariant in time within the time window of size T_w. The objective function to be minimized is:

$$\mathcal{J}(\delta\mathbf{u}) = \sum_{i=1}^{N_f} \sum_{m=1}^{\lfloor T_w/\Delta t \rfloor} \left\| \mathbf{r}_i^{\,b}(\mathbf{u}_m^b) + \delta\mathbf{r}_i(\delta\mathbf{u}) - \mathbf{r}_{i,m}^{\mathrm{obs}} \right\|^2 + \alpha_1 \left\|\delta\mathbf{u}\right\|_{\mathbf{B}}^2 + \alpha_2 \sum_{j,k} (\nabla \cdot \delta\mathbf{u})^2, \tag{4}$$

where N_f is the number of drifters, i is the index of the drifter and Δt is the sampling time of the observations. $\mathbf{r}_{i,m}^{\mathrm{obs}}$ represents the observed position of drifter i at time $m\Delta t$. The term $\mathbf{r}_i^{\,b}$ (resp. $\delta\mathbf{r}_i$) is the position of the drifter i estimated by an advection model calculated from the background field $\mathbf{u}_m^b$ (resp. from the incremental correction $\boldsymbol{\delta}\mathbf{u}$). The advection model consists of a numerical integration of the advection equation, for example, using an Euler scheme. The first term measures the misfit between the observations and the positions of drifters simulated considering the advection by the surface velocity field. The second component requires the corrected field to stay close to the background velocity. Here the $\mathbf{B}$-norm is defined as $\|\psi\|_{\mathbf{B}}^2 \equiv \psi^T \mathbf{B}^{-1} \psi$, where $\mathbf{B}$ is the error covariance matrix. The error covariance matrix $\mathbf{B}$ is obtained using the diffusion filter method of Weaver and Courtier (2001). The choice of the length scale R of the correction that enters in the error covariance matrix can be done in the context of the sensitivity analyses. The last component is a constraint on the geostrophic part of the velocity, required to stay divergence free. This term is added to ensure a physical correction, avoiding artifacts especially near the coasts. The weights α_1 and α_2 correspond to the confidence given to the respective terms of the cost function, relative to the observation error term. Because the cost function is defined within a multiplicative constant, it is safe to set a standard confidence of one to the observation error term, assuming that each observation error is equal and de-correlated from the other. The relative confidence in the background α_1, and in the non-divergent constraint α_2 cannot be objectively determined. So they are determined empirically using sensitivity analyses (see Section 3.1). After the minimization, we compute a corrected velocity field:

$$\mathbf{u}_{\mathrm{m}}^{\mathrm{corr}} = \mathbf{u}_m^b + \delta\mathbf{u} \tag{5}$$

Because $\delta\mathbf{u}$ is constant inside a time window and to obtain a smooth, time-dependent velocity field, a sliding window T_w, of time shift σ is used to obtain smoother corrections in time. A detailed description of the algorithm is found in Issa et al. (2016).

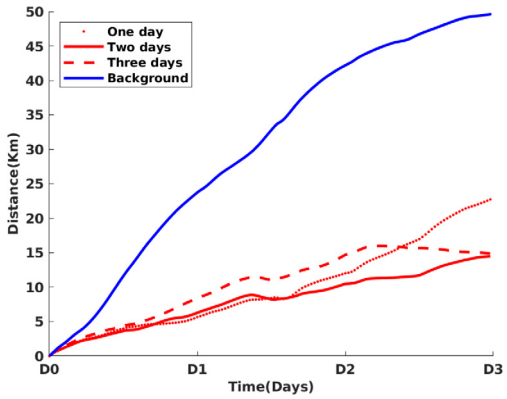


Fig. 2. Distance variation $d(t)$ as in Eq. (6) between the simulated positions and real observations. The red lines represent the simulations after assimilation using a temporal window size T_w of one, two, and three days. The blue line represents the distance between the observed drifter and the one simulated by the background velocity field.

3.1. Sensitivity tests

Sensitivity tests allow to tune the following parameters of the algorithm: the temporal size of the window (T_w), the divergence coefficient (α_2) and the length scale R of the correction that enters in the error covariance matrix. In Fig. 10, we show the setup of the sensitivity experiment: three drifters were circulating close to each other near the Libyan coast. Two drifters, shown in colors, are assimilated to produce a corrected velocity field. The resulting corrected velocity field is used to simulate the trajectory of the third independent drifter (shown in black). The metric used is the mean separation distance between the simulated and observed trajectories:

$$d(t) = \frac{1}{N_w} \sum_{j=1}^{N_w} \|\mathbf{r}_j(t) - \mathbf{r}_j^{obs}(t)\|^2, \tag{6}$$

where N_w is the number of windows used during the simulation.

Temporal window sizes T_w of 1, 2, and 3 days were compared. Fig. 2 reveals that a window size of 2 days maximally reduces distances. The improvement reaches around 70% compared to the background, 5% and 9% more when compared to T_w of 1 and 3 days respectively. To produce a smooth time-dependent velocity, we use a sliding window of time-shift σ. We opted for σ of half a day to have a smoother correction.

The other two parameters seem not to have a significant impact on the assimilation. For example, if the value of α_2 is changed from $5{\times}10^{-6}$ to null, the solution is modified by only around 0.7%. For the length scale parameter, varying R from 20 to 30 km improves the correction by around 3% only.

Consequently, in the further experiments we apply the algorithm with the following parameters: $T_w = 2$ days, σ = half-day, $\alpha_2 = 5{\times}10^{-6}$, and R = 30 km.

4. Validation method

4.1. Current meter

On the 1st of June 2006, the 1st selected drifter (OGS drifter identification number: 3627) circulated near the C_3 mooring at a distance shorter than 30 km. This passage allows us to apply the algorithm to the area containing C_3. The drifter trajectory is assimilated starting from this day, denoted by D_0. The experiment extends until the 14th of June (D_{13}).

The current meter was fluctuating around 73 m deep during the drifter passage, as is revealed by its pressure reading. On the other hand, drifters track the current at ~15 m. To assess the validity of the comparison with these two different depths, we computed the temporal

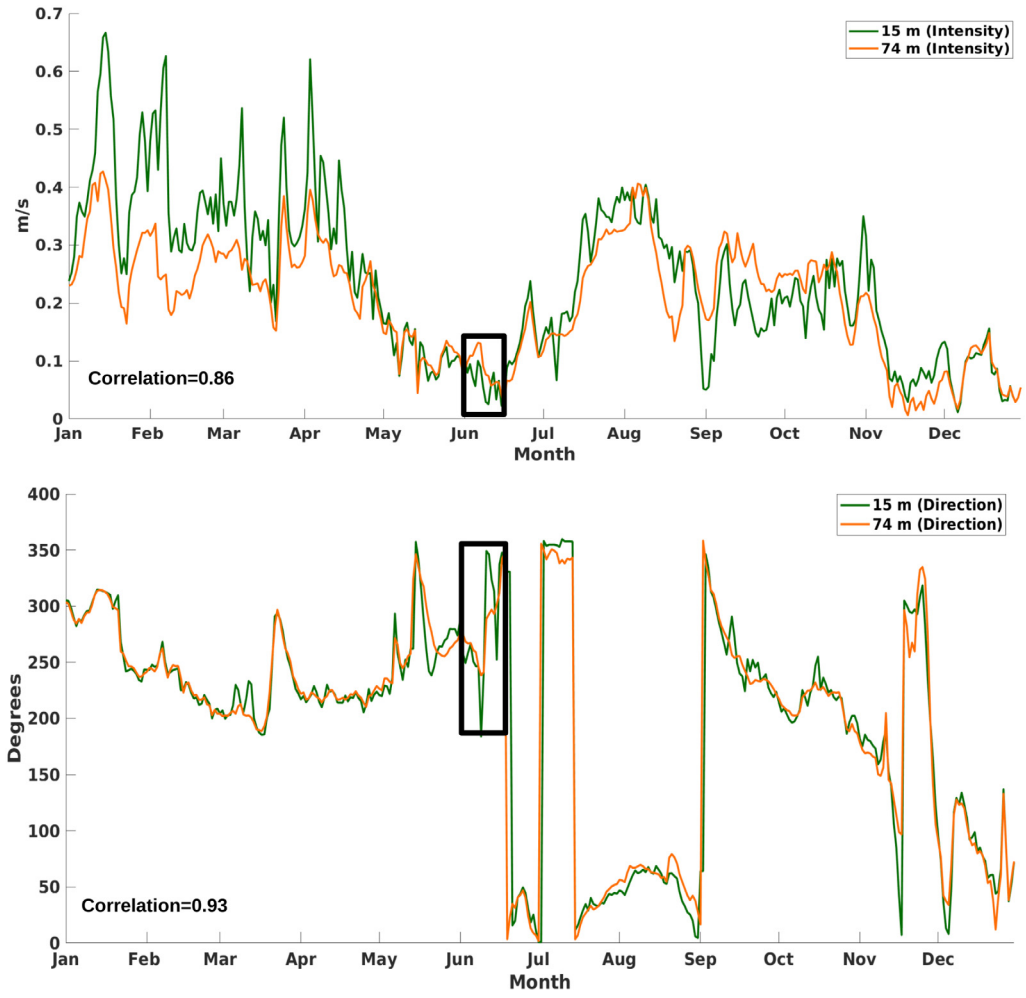


Fig. 3. Temporal variations of the current velocity (upper panel) and the direction (lower panel) at 74 (orange) & 15 m (green) depth, as shown by MFS. The period of the experiment (1–14 Jun 2006) is indicated by the black rectangle.

variation of the velocity field (intensity and angle) at both depths using the products derived from the Mediterranean Forecasting System.

The variation of the intensity and direction of the current in the year 2006 is presented in Fig. 3 at 15 m and 74 m depth. It includes the days of the experiments dating from the 1st and the 14th of June. The jumps in the direction (from mid-June, until mid-July) are due to the periodic definition of the direction. During the experiment, the difference between the velocities at the two depths is 0.033 m/s on average (with a standard deviation of 0.074 m/s); the difference in the direction is $\sim 0.3°$ on average (with a standard deviation of 37°). These differences are small compared with the natural variability of the signal (standard deviation of 0.23 m/s for the velocity and 97° for the angle). Moreover, there is a high correlation existing between both levels, with a correlation of 0.93 for the direction and 0.86 for the intensity.

It should be mentioned that the mixed layer was not deep enough to include the current meter ~ 70 m depth, so the comparison between the drifter and the current meter underneath could induce a bias. However, as discussed above, the MFS results show the currents at the two different depths agree well in terms of direction and intensity during the time of the experiment. Thus, the current meter measurements at 73 m depth can still be used to validate the corrected surface velocity estimated at 15 m depth.

Let us denote the current meter velocity by $\mathbf{u}_m^{\text{ref}}$, and use $\mathbf{u}_m$ for the fields associated with the assimilation experiment (either the background or the corrected one). The zonal and meridional components are: $\mathbf{u}_m^{\text{ref}} = (u_m^{\text{ref}}, v_m^{\text{ref}})$, and $\mathbf{u}_m = (u_m, v_m)$. Similarly, we use θ^{ref} for the current-meter velocity angle variation and θ for either the background or the corrected velocities.

For an overall quantification of the assimilation impact, we calculated the L_2 norm error between $\mathbf{u}_m^{\text{ref}}$ and $\mathbf{u}_m$ velocity fields.

$$E_m = \sqrt{(u_m^{\text{ref}} - u_m)^2 + (v_m^{\text{ref}} - v_m)^2}. \tag{7}$$

Low values of E_m^2 reveal a similarity in both intensity and direction between the compared vectors.

4.2. Comparison with glider

A drifter from the NEMED project was circulating close to a glider providing geostrophic velocities perpendicular to its trajectories. We use the glider-derived velocities ($\mathbf{u}_m^{\text{ref}}$), averaged between 0 and 20 m, as observations to be compared with the experimented velocity fields ($\mathbf{u}_m$). The experimented velocities are interpolated and orthogonally projected to the glider trajectory as explained in the data section.

To assess the assimilation efficiency, we compute the average error (E_a) between the projected experimented velocities and the glider-derived velocities.

$$E_a = \frac{1}{M_g}\left(\frac{\sum_{m=1}^{m=M_g} \|\mathbf{u}_m\| - \|\mathbf{u}_m^{ref}\|}{\sum_{m=1}^{m=M_g} \|\mathbf{u}_m^{ref}\|}\right) \times 100, \tag{8}$$

where M_g represents the total glider positions used for comparison, $\|\mathbf{u}_m\|$ the norm of the background and assimilated projected velocities at each glider position and $\|\mathbf{u}_m^{ref}\|$ represents the glider-derived velocities norm at each position.

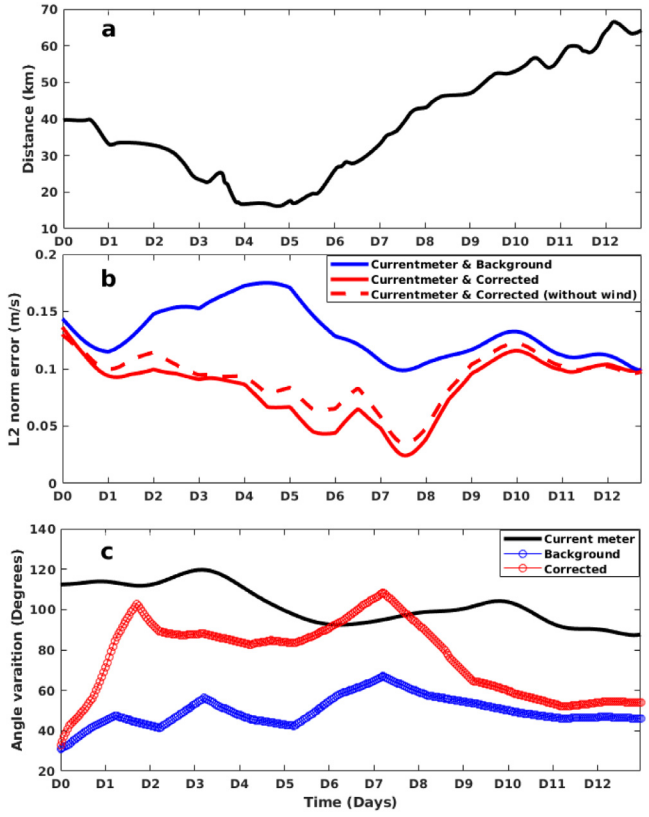


Fig. 4. The upper panel shows the distance evolution between the drifter and the current meter C_3 location. The middle panel shows the L_2 norm error variation of the background (blue) compared to the corrected velocity field with (solid) and without (dashed) adding the ageostrophic component during the assimilation. The lower panel represents the time series of the current direction as derived from the current meter C_3 (black line), the background (blue line), and the corrected (red line) currents.

4.3. Comparison with ocean color data

A drifter that was circulating in a high vorticity area is assimilated from the 1st of February 2006 until 28th of June 2006. The mesoscale structure trapping the drifter was also well defined in terms of shape and location by a contemporary chlorophyll image. A visual observation of the eddy is possible by drawing the streamlines resulting from the background and assimilated velocity fields. So the eddy shape could be represented by the flow lines of the resulting velocity fields. A better agreement with the eddy as observed from the chlorophyll image is expected after correction (in terms of shape and location).

5. Results

In this section we show all the results of the comparisons from the background, the corrected velocity field and the independent current measurements derived from different sources (current meter, glider, ocean color, drifters).

5.1. Comparison with current meter

The first comparison focused on the area off the Libyo-Egyptian coast (see Fig. 1).

In the period between the 1st (D0) and the 14th (D13) of June 2006, the drifter 57306 (Argos number), that collects data close to and concurrently to the C3 current meter, is selected for the assimilation.

Fig. 4c shows the temporal variation of the current direction as recorded by C_3. This change in the angle current direction of C_3 was then compared to the variations of the background and corrected velocity fields. Significant improvements are seen starting from D_0 until D_{12}. During this period, the direction of the corrected velocity is close to the one measured by C_3. Furthermore, the improvement in direction reaches more than 40 degrees after correction, especially between D_2 and D_8. A significant shift in the current direction is detected between D_0 and D_2, varying from 60 to 140 degrees within only a few hours during these dates. This adjustment corresponds to the time when the drifter gets closer to C_3, from ~ 40 to ~ 30 km (see Fig. 4a).

Fig. 4b confirms the previous results and demonstrates how the assimilation reduces the overall L_2 error. This error is reduced after correction starting from D_0. During D_4, and D_5, the largest improvement from the background is observed. In fact, the amplitude of the corrections depends on two main factors: the initial error of the background and the distance between the drifter and the point of interest (here the C_3 location). The difference between the background and the corrected velocity field increases with decreasing distances. When the drifter gets far away again (>30 km), the impact of the assimilation diminishes progressively.

Excluding the ageostrophic component from the background during the assimilation does not have a significant impact on the resulting corrected velocity field. As Fig. 4b shows, adding the wind component to the background velocity slightly reduces the overall $L2$ error between the corrected and current-meter velocity fields. During the experiment, the wind forcing was oriented towards the South-Southeast and had an average speed of 7 m/s.

The average velocity field during the days of the experiments (from D_0 until D_{12}) is presented in Fig. 5. After the drifter passage, the resulting assimilated velocity vectors (red vectors) are modified in a way that is consistent with the mean-field recorded by the current meter (dark vector).

Fig. 6 shows the daily average velocity field on the $4^{th}(D_3)$, $6^{th}(D_5)$, $8^{th}(D_7)$, $12^{th}(D_{11})$ of June 2006. On D_3, when the circulating drifter is still far from the current meter location, the corrected velocity field near C_3 is close to the background. Both velocity fields are different from the current meter. The average current as recorded by C_3 is oriented to the North-Northwest, while both velocity fields are oriented North-Northeast. In D_5 when the drifter gets closer to C_3, an important shift of the corrected velocity field vectors is noticed. The agreement between the C_3 and the corrected current vectors improves, up to the best match on D_7. In D_{11}, when the drifter becomes distant, there is no more impact of the correction on the velocity field around C_3. As a result, the background and the assimilated velocity fields are again similar.

5.2. Comparison with glider

We targeted a drifter from the Surface Circulation in the Northeastern Mediterranean (NEMED) project releasing drifters between Cyprus and the Middle East from summer 2009 to spring 2010.

Fig. 7a shows that starting from December 3rd (the glider deployment date) and until the 21st of December 2006, there was a drifter circulating near the deployment location in the South of Cyprus. Although they were many intersections between the glider and drifter trajectories, most of these intersections occurred at different times. Only between the 10th and 11th of December 2009, the TRIESTE-1 glider circulated at a distance less than 30 km with the drifter 92060 (see red square). We assimilate the latter, and obtain corrected velocities around the glider location.

The glider surfaces approximately every hour, with three observations starting from 7 pm on the 10th and seventeen observations on the 11th. That is a total of twenty observations during these two days (Fig. 7b). The background and the assimilated velocity fields are then interpolated at these glider positions (P). Because the derived geostrophic velocities are perpendicular to the glider trajectory, the interpolated background and assimilation are orthogonally projected onto the glider trajectory.

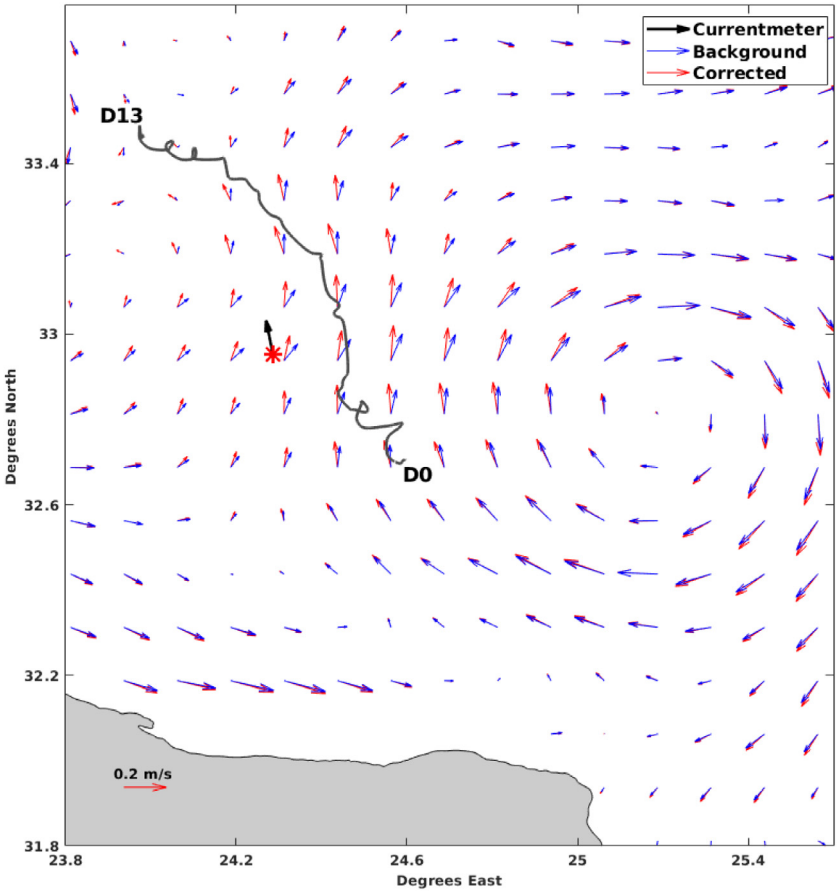


Fig. 5. Average velocity field during the 14 days of the experiment between the 1st and the 14th of June 2006. The drifter trajectory is represented by the solid black line moving from the South to the North. The black vector represents the average current recorded by C_3 (represented by the red star).

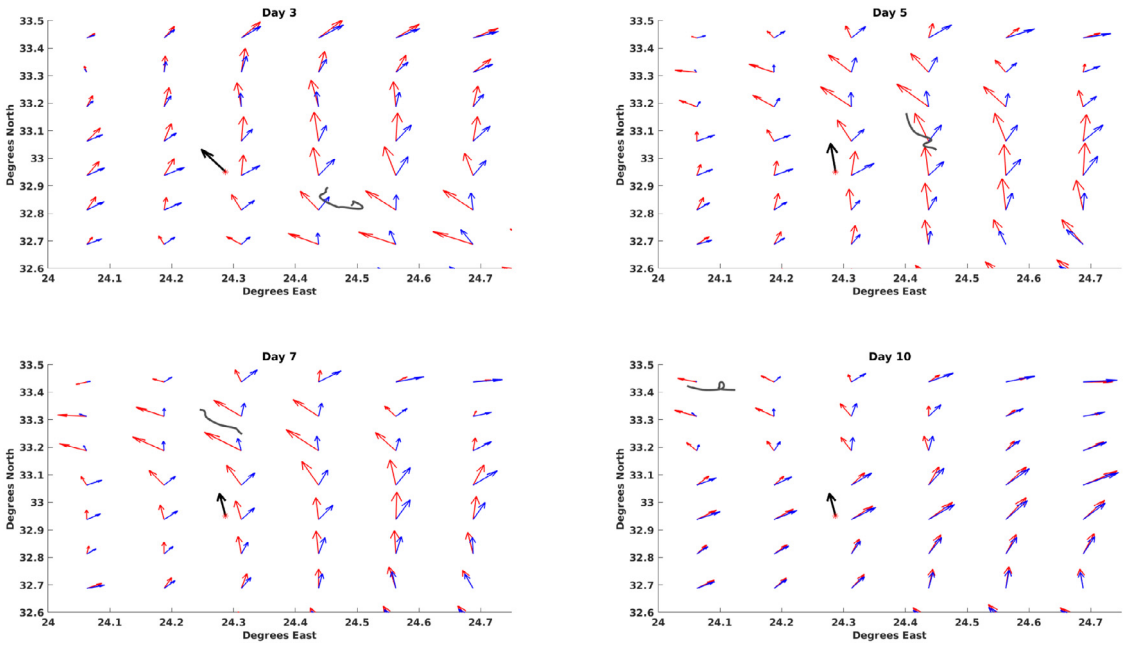


Fig. 6. The daily average velocity field on the 4th, 6th, 8th, 12th of June 2006 of the current meter C_3 (black), the background (blue) and the corrected (red) together with the drifter trajectory (black curve).

In Fig. 7c, we show the background and corrected fields, together with the velocity computed using the glider data. It can be seen that the projected velocity norm shows how the background tends to underestimate the intensity with a maximum value reaching 0.08 m/s. After correction, the resulting velocity norm increases. When we compare it with the glider results (around 0.14 m/s), the corrected

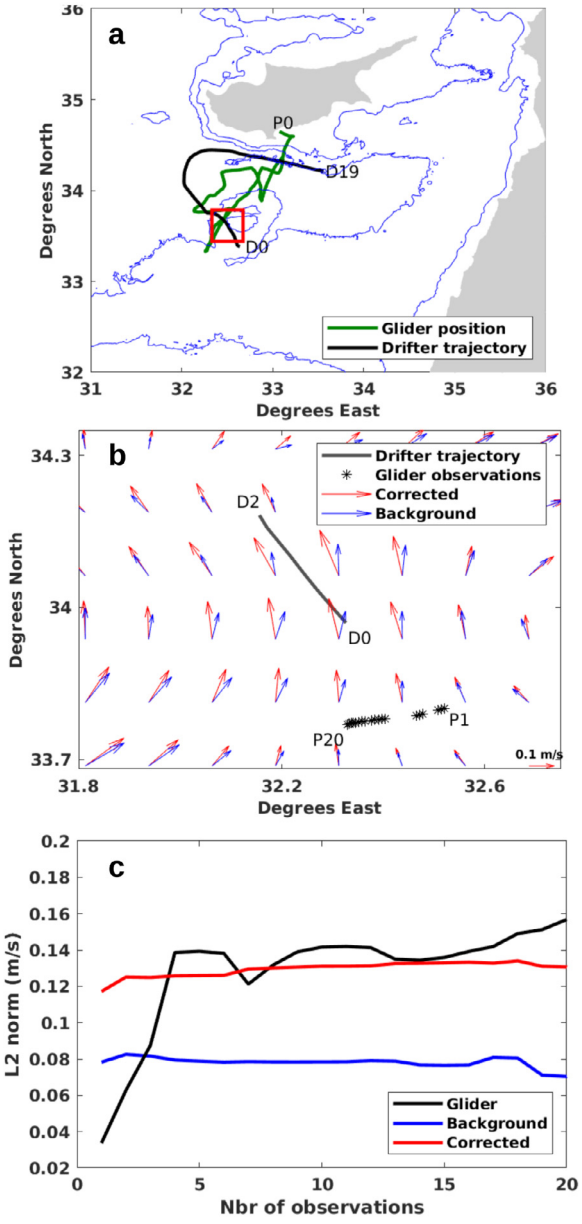


Fig. 7. Glider (green) and drifter (dark) trajectories between the 10th and 11th of December 2009. The red rectangle represents the location where the intersection between the glider and drifter trajectories is contemporary. The two days of the glider passage near the drifter are schematized in the middle panel. The glider positions are represented by black stars. All of this is overlaid on the average velocity field of the background and the assimilation. The lower panel represents average velocity norm of the vectors orthogonally projected at the glider positions of the background (blue) and the corrected (red) velocity field. They are compared with the glider-derived velocity norm (dark).

values are closer (0.12 m/s) than the background values (0.08 m/s). The overall error E_a has been reduced by more than 20% by the assimilation. This improvement is important despite two factors that could tend to penalize the assimilation. First, the different time scale of observation, where the sampling time of the gliders is hourly while the sampling frequency of the drifter is every six hours. The second factor is the distance between the assimilated drifter and the observed glider positions (P). The distance between the nearest sample drifter position and P1 is more than 25 km. This distance increases continuously and reduces the correction impact.

5.3. Comparison with high resolution ocean color images

We targeted a drifter (Argos number: 57307) that was released in 20.85°E, 33.055°N from the 1st of February 2006 until 28th of June 2006. This drifter was stuck in one of the highly active eddies off the Egyptian coasts (see Fig. 8) for several weeks starting May 17, 2006. A contemporary chlorophyll image was available during this period, specifically on May 20, showing the eddy shape and location.

The assimilation experiment was done for 6 days, starting from the 17th of May. The streamlines of the velocity fields before and after correction were compared with the simultaneous chlorophyll-a concentration image in Fig. 9. The observed streamlines of the velocity field after correction (red) are close to the chlorophyll-a image in terms of shape and location, while the background velocity field presents a shift in location and difference in size. The latter reveals an extension of the eddy towards the southeast.

5.4. Reconstruction of independent drifter trajectory

As explained in Section 3.1, we used three drifters trapped in the anticyclone noted LE1 off Libya (see Figs. 2 and 5 in Gerin et al. (2009); see also Fig. 1 in Sutyrin et al. (2009)). Between the 8th and the 27th of May 2006, we assimilated the positions of the Argo numbers 59777 and 59774 to simulate the position evolution of the third one (57312) based on the surrounding velocity field (see Fig. 10).

The prediction of the future drifter positions after correcting the velocity field is closer to the real trajectory during the 20 days of the experiment (as shown in Fig. 11). Predicted positions after correction (in red) reveal trends that are similar to the real ones. On the other hand, predictions based on the background velocities differ from the real observations as they do not show circular patterns.

The lower panel presents the evolution in time of the distance $d(t)$ as in Eq. (6), between the observed position and the simulated position of the independent drifter before and after correction. The simulated drifter position is reinitialized every 2 days to the position of the real drifter. The distance is computed for each of these 2 days windows (T_w) and then averaged to produce the average position error in time. Fig. 11 shows a decrease of this error after the correction. The distance between the expected and the real observation reaches around 40 km using the background velocities. The assimilation reduces these distances to less than 9 km. Moreover, the correction lowers the uncertainties (standard deviation of the error over each of the 10 windows) as compared to those of the background (see Fig. 11). The standard deviation of the background distances increases continuously with time reaching more than 19 km at the end of the window after two days. After correction, these variations are significantly reduced and barely increase with time, and do not exceed 3.7 km. In other words, on average, the assimilation allows us to reduce the error from 40 to less than 9 km after two days when simulating the positions of independent drifter not included in the assimilation.

6. Perspectives

When in-situ drifters data are available, the assimilation could be applied on a larger spatio-temporal scale. From all the 97 drifters of the EGYPT/EGITTO campaign, 29 drifters covering the area between the Libyo-Egyptian coasts and Crete (between ~21° to ~31°E, and ~30° to ~36°N in 2006 have been assimilated. In general, altimetry strongly underestimates the Mean Kinetic energy (MKE) and Eddy Kinetic Energy (EKE) of the velocity field (Pujol and Larnicol, 2005; Gerin et al., 2009; Poulain et al., 2012). So we expect the assimilation to improve those estimates obtained from altimetry. Fig. 12 reveals that the MKE increases after assimilation, especially when targeting a main regional mesoscale feature such as Ierapetra eddy (IE) (Amitai et al., 2010; Ioannou et al., 2017). After correction, the MKE in IE is more than 700 cm^2/s^2 on all sides with a maximum of ~760 cm^2/s^2. For the

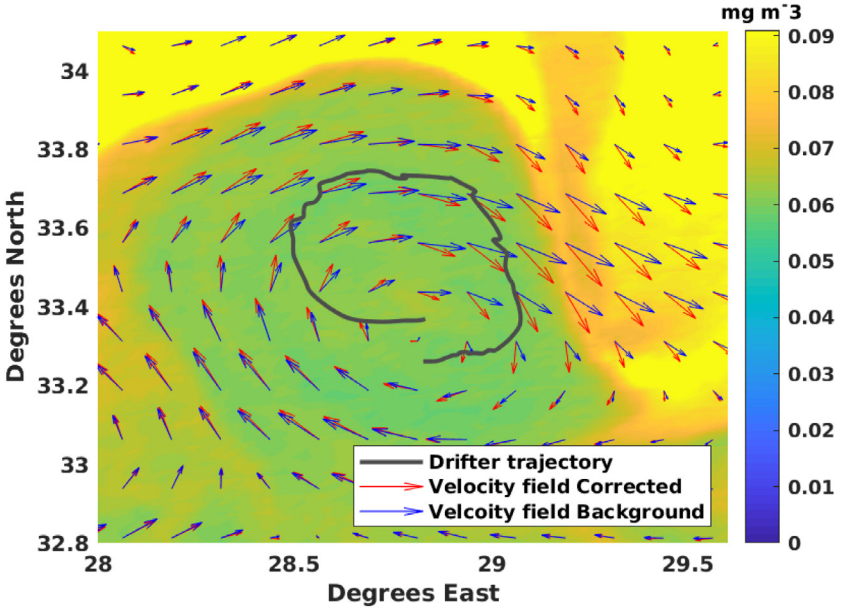


Fig. 8. Average of the background (blue) and the corrected (red) velocity fields after six days of assimilation starting from the 17th of May 2006. Drifter trajectory is represented in gray. All of them are overlaid on a high-resolution chlorophyll-a image of 20 May 2006.

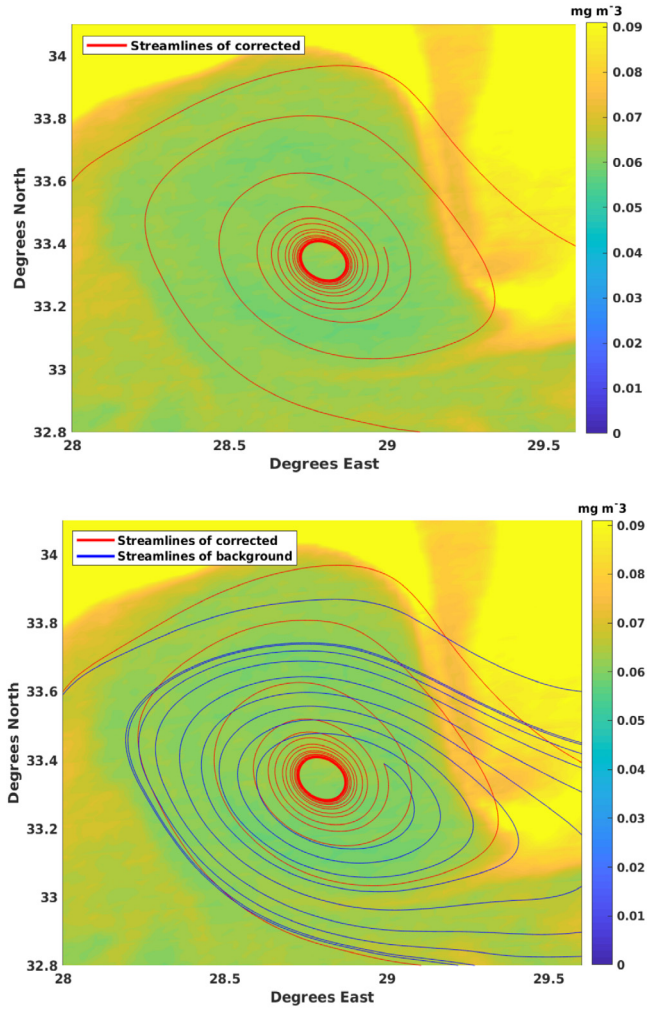


Fig. 9. Velocity field streamlines after correction (upper panel) compared with the background (lower panel) overlaid on chlorophyll-a image of 20 May 2006.

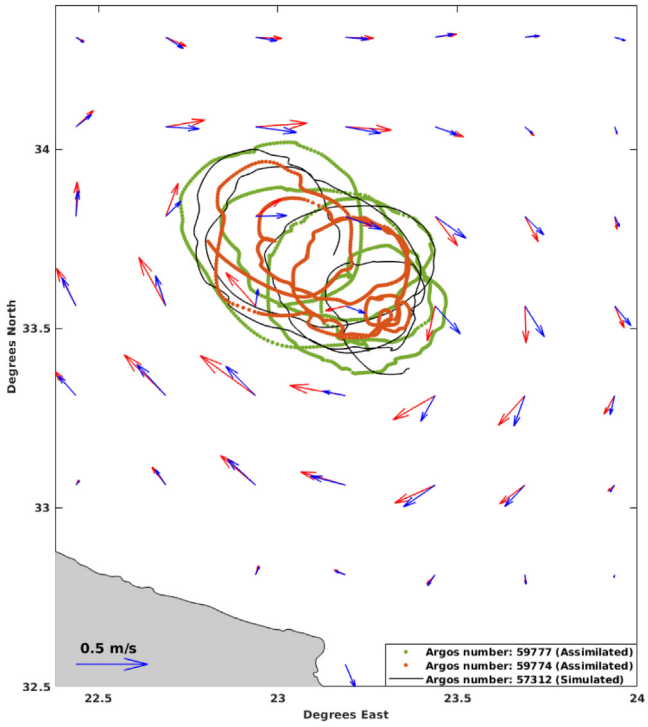


Fig. 10. The trajectory of the three drifters circulating close to each other between 8th and the 27th of May 2006. The dark line represents the real trajectory of the non-assimilated drifter, while the lines in green and orange represent the trajectories of the assimilated drifters. These trajectories are overlayed on the resulting average velocity field before (blue) and after assimilation (red).

background, MKE reaches a maximum of ~630 cm^2/s^2 but only locally. The eastern and the western sides of the eddy have low values of MKE as they do not exceed ~350 cm^2/s^2.

Moreover, EKE (see Fig. 13) reveals a higher variability after assimilation, especially in the Ierapetra area and near the Libyan coast. After assimilation, all sides of the IE structure reach more than 500 cm^2/s^2 with a maximum of ~1100 cm^2/s^2. For the background, values over

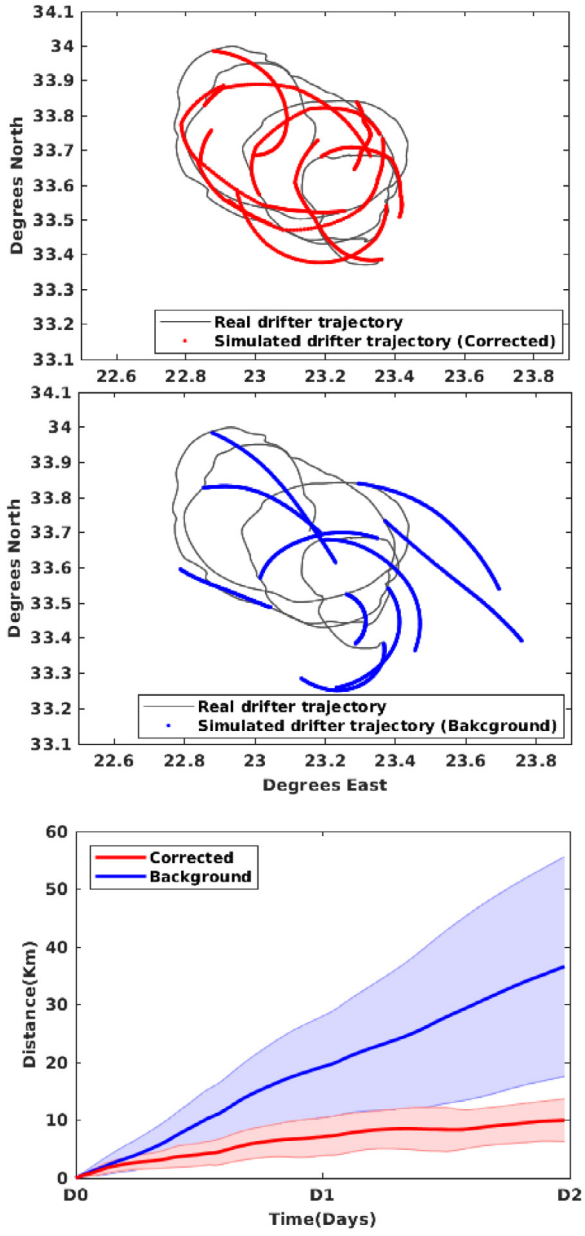


Fig. 11. The red lines (blue) represent the simulated drifter position using the corrected (background) velocity field. Both trajectories are compared with the real observations (dark). In the lower panel, the red (blue) line represents the distance evolution ($d(t)$ as in Eq. (6)) between the simulated trajectory using the corrected field (background) and the real observations, averaged over 10 simulations. Shades around the lines represent the standard deviation over the 10 simulations.

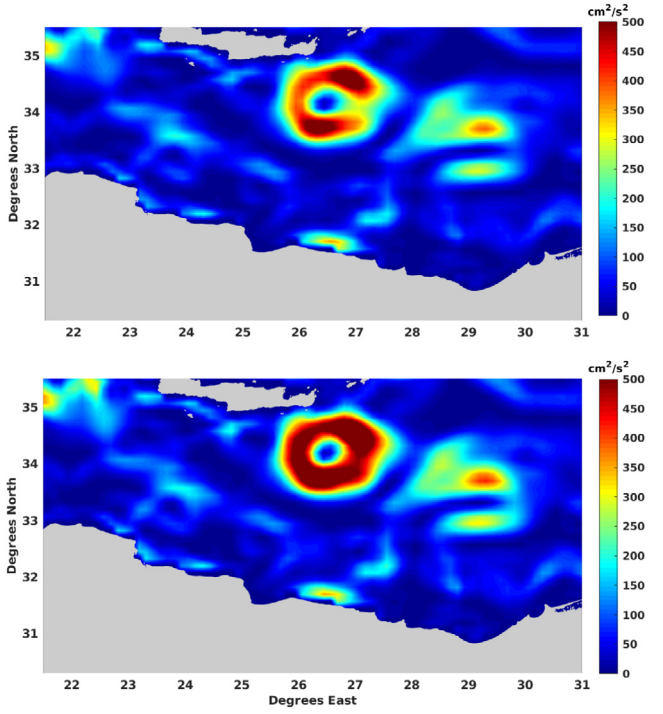


Fig. 12. The annual Mean Kinetic Energy (MKE) in 2006 resulting from background (upper panel) and the assimilated velocity fields (lower panel).

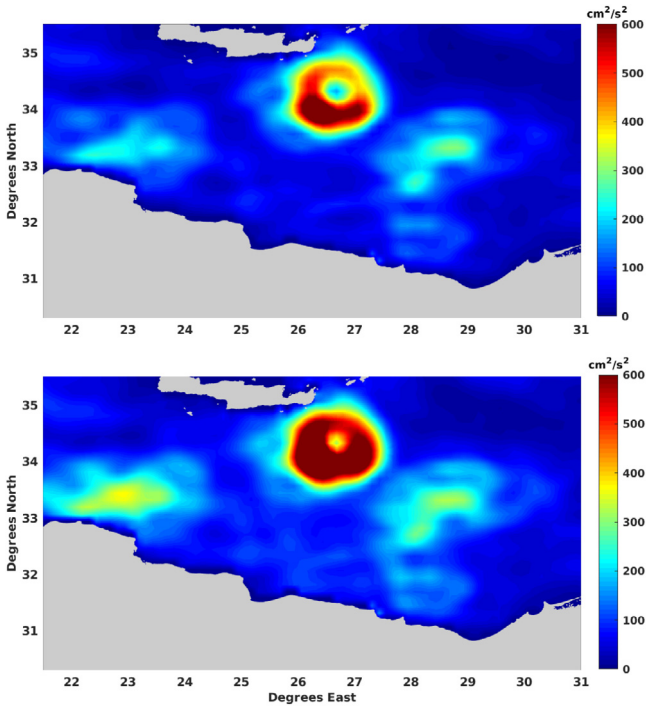


Fig. 13. The annual Eddy Kinetic Energy (EKE) in 2006 resulting from background (upper panel) and the assimilated velocity fields (lower panel).

500 cm^2/s^2 are limited to the southern part of IE with a maximum of ~860 cm^2/s^2.

The differences in MKE and EKE reveal that the algorithm can help in revising the quantification of surface velocity features, mainly in the Ierapetra area and off the Libyan coast, where intense mesoscale features are found permanently. A further detailed study of these areas based on this method could help investigate some oceanographic questions that are unclear, especially off Libya where the Libyo-Egyptian Current generates instabilities and thus a very high variability which paves the way to differing interpretations.

7. Conclusion

This paper has extended the application and objectively validated the assimilation algorithm developed in Issa et al. (2016). When compared with in-situ contemporary current meter data located in the assimilated area, the modified velocity field is in better agreement with

the current meter records. Significant improvements are seen when the assimilated drifter reaches a distance less than 30 km from the current meter location. This spatial extension of correction is larger than the internal Rossby radius in the Mediterranean that is on the order of 10–14 km (Robinson et al., 2001). We have shown that the corrected velocity field is closer to current meter data in both direction and intensity.

The application of the assimilation in high vorticity areas gives more realistic results than the altimetric product. After assimilating drifter positions trapped in an eddy detected at the same time from high-resolution chlorophyll images, the resulting streamlines from the corrected velocity field are consistent with the eddy shape and location, as shown by the ocean color image.

To quantify the assimilation efficiency, we showed that the error between the real and simulated drifter positions decreases after assimilation, from 40 km without assimilation to less than 10 km with assimilation after two days. Also, the correction reduces the uncertainties during all the experiments.

Further to the East, gliders from the "Eye of the Levantine" campaign deployed in the south of Cyprus were used for further validation. The resulting perpendicular velocity norm has values closer to the glider-derived velocities after assimilation. Despite the difference in the sampling time-scale and the considerable distances, the assimilation was able to reduce the error by more than 20%.

The results obtained pave the way for further investigations and larger spatio-temporal applications in the Eastern Mediterranean, where many drifter positions are available. This application can provide a precise and detailed description, improving the understanding of the mesoscale and sub-mesoscale activity.

CRediT authorship contribution statement

Georges Baaklini: Writing – original draft, Software, Formal analysis, Visualization. **Leila Issa:** Conceptualization, Methodology, Writing – review & editing, Project administration, Validation, Supervision. **Milad Fakhri:** Funding acquisition, Writing – review & editing, Supervision. **Julien Brajard:** Conceptualization, Methodology, Writing – review & editing, Project administration, Validation, Supervision. **Gina Fifani:** Software, Writing – review. **Milena Menna:** Writing – review & editing, Resources. **Isabelle Taupier-Letage:** Writing – review & editing, Resources. **Anthony Bosse:** Writing – review & editing, Resources. **Laurent Mortier:** Conceptualization, Funding acquisition, Writing – review & editing, Validation, Supervision.

Declaration of competing interest

The authors declare that they have no known competing financial interests or personal relationships that could have appeared to influence the work reported in this paper.

Acknowledgments

We would like to acknowledge the National Council for Scientific Research of Lebanon (CNRS-L) for granting a doctoral fellowship to Georges Baaklini. This work was partially funded by the ALTILEV program in the framework of the PHC-CEDRE project. We would like to thank Professor Alexandre Stegner (CNRS) for helping in data interpretation.

Drifters data were provided from: doi:data/10.6092/7a8499bc-c5ee-472c-b8b5-03523d1e73e9. We thank Pierre-Marie Poulain (CMRE) for his contribution in providing the drifters data.

EGYPT/EGITTO(Eddies and GYres Paths Tracking) program received funding from CNRS INSU LEFE IDAO and Mercator programs

Glider data are available on http://www.ifremer.fr/co/ego/ego/v2/trieste-1/trieste-1_20091124/. They were collected and made freely available by the Coriolis project and programmes that contribute to it (http://www.coriolis.eu.org)

The altimeter products were produced by Ssalto/Duacs and distributed by AVISO, with support from CNES (http://www.aviso.altimetry.fr/duacs/).The drifter data are distributed by OGS (http://nodc.ogs.trieste.it/). Chlorophyll image was provided by NASA Goddard Space Flight Center, Ocean Ecology Laboratory, Ocean Biology Processing Group. Moderate-resolution Imaging Spectroradiometer (MODIS) Aqua Chlorophyll Data; 2018 Reprocessing. NASA OB.DAAC, Greenbelt, MD, USA. doi:data/10.5067/AQUA/MODIS/L3B/CHL/2018.

The MIO has received funding from European FEDER Fund under project 1166–39417.

Bathymetry data are provided by GEBCO Compilation Group (2020) GEBCO 2020 Grid (doi:10.5285/a29c5465-b138-234d-e053-6c86abc040b9).

Appendix

If u and v are the zonal and meridional velocities respectively, the Mean Kinetic Energy (MKE, cm^2/s^2) is computed:

$$MKE = \frac{1}{2}\left(|u|^2 + |v|^2\right)$$

where $|\ |$ is the time averaging of the component in a given bin.

The Eddy Kinetic Energy (EKE) is:

$$EKE = \frac{1}{2}\left(|u'u'| + |v'v'|\right)$$

$|u'u'|$ and $|v'v'|$ are the variances in the zonal and meridional directions, respectively.

References

Amitai, Y., Lehahn, Y., Lazar, A., Heifetz, E., 2010. Surface circulation of the eastern Mediterranean Levantine basin: Insights from analyzing 14 years of satellite altimetry data. J. Geophys. Res. Oceans 115 (C10).

Amores, A., Jordà, G., Arsouze, T., Le Sommer, J., 2018. Up to what extent can we characterize ocean eddies using present-day gridded altimetric products? J. Geophys. Res. Oceans 123 (10), 7220–7236.

Berta, M., Griffa, A., Magaldi, M.G., Özgökmen, T.M., Poje, A.C., Haza, A.C., Olascoaga, M.J., 2015. Improved surface velocity and trajectory estimates in the Gulf of Mexico from blended satellite altimetry and drifter data. J. Atmos. Ocean. Technol. 32 (10), 1880–1901.

Bosse, A., Fer, I., 2019. Mean structure and seasonality of the Norwegian Atlantic Front Current along the Mohn Ridge from repeated glider transects. Geophys. Res. Lett. 46 (22), 13170–13179.

Caballero, I., Gómez-Enri, J., Cipollini, P., Navarro, G., 2013. Validation of high spatial resolution wave data from Envisat RA-2 altimeter in the Gulf of Cádiz. IEEE Geosci. Remote Sens. Lett. 11 (1), 371–375.

Carrier, M.J., Ngodock, H., Smith, S., Jacobs, G., Muscarella, P., Ozgokmen, T., Haus, B., Lipphardt, B., 2014. Impact of assimilating ocean velocity observations inferred from Lagrangian drifter data using the NCOM-4DVAR. Mon. Weather Rev. 142 (4), 1509–1524.

Cipollini, P., Benveniste, J., Bouffard, J., Emery, W., Gommenginger, C., Griffin, D., Høyer, J., Madsen, K., Mercier, F., Miller, L., et al., 2010. The role of altimetry in coastal observing systems. Proc. OceanObs 9, 181–191.

Dee, D.P., Uppala, S.M., Simmons, A., Berrisford, P., Poli, P., Kobayashi, S., Andrae, U., Balmaseda, M., Balsamo, G., Bauer, d.P., et al., 2011. The ERA-Interim reanalysis: Configuration and performance of the data assimilation system. Q. J. R. Meteorol. Soc. 137 (656), 553–597.

d'Ovidio, F., Fernández, V., Hernández-García, E., López, C., 2004. Mixing structures in the Mediterranean Sea from finite-size Lyapunov exponents: Mixing structures in the Mediterranean Sea. Geophys. Res. Lett. 31 (17), http://dx.doi.org/10.1029/2004GL020328, URL: http://doi.wiley.com/10.1029/2004GL020328.

Eriksen, C.C., Osse, T.J., Light, R.D., Wen, T., Lehman, T.W., Sabin, P.L., Ballard, J.W., Chiodi, A.M., 2001. Seaglider: A long-range autonomous underwater vehicle for oceanographic research. IEEE J. Ocean. Eng. 26 (4), 424–436.

Escudier, R., Mourre, B., Juza, M., Tintoré, J., 2016. Subsurface circulation and mesoscale variability in the Algerian subbasin from altimeter-derived eddy trajectories: Algerian Eddies propagation. J. Geophys. Res. Oceans 121 (8), 6310–6322. http://dx.doi.org/10.1002/2016JC011760, URL: http://doi.wiley.com/10.1002/2016JC011760.

Gerin, R., Poulain, P.-M., Taupier-Letage, I., Millot, C., Ben Ismail, S., Sammari, C., 2009. Surface circulation in the Eastern Mediterranean using drifters (2005–2007). Ocean Sci. 5 (4), 559–574. http://dx.doi.org/10.5194/os-5-559-2009, URL: https://os.copernicus.org/articles/5/559/2009/.

Hamad, N., Millot, C., Taupier-Letage, I., 2006. The surface circulation in the eastern basin of the Mediterranean Sea. Sci. Mar. 70 (3), 457–503.

Hayes, D., Zodiatis, G., Konnaris, G., Hannides, A., Solovyov, D., Testor, P., 2011. Glider transects in the Levantine Sea: Characteristics of the warm core Cyprus eddy. In: OCEANS 2011 IEEE-Spain. IEEE, pp. 1–9.

Ioannou, A., Stegner, A., Le Vu, B., Taupier-Letage, I., Speich, S., 2017. Dynamical evolution of intense Ierapetra eddies on a 22 year long period. J. Geophys. Res. Oceans 122 (11), 9276–9298.

Issa, L., Brajard, J., Fakhri, M., Hayes, D., Mortier, L., Poulain, P.-M., 2016. Modelling surface currents in the Eastern Levantine Mediterranean using surface drifters and satellite altimetry. Ocean Model. 104, 1–14.

Kamachi, M., O'Brien, J., 1995. Continuous data assimilation of drifting buoy trajectory into an equatorial Pacific Ocean model. J. Mar. Syst. 6 (1–2), 159–178.

Kubryakov, A., Stanichny, S., 2011. Mean dynamic topography of the black sea, computed from altimetry, drifter measurements and hydrology data. Ocean Sci. 7 (6), 745.

Laxenaire, R., Speich, S., Blanke, B., Chaigneau, A., Pegliasco, C., Stegner, A., 2018. Anticyclonic eddies connecting the western boundaries of Indian and Atlantic Oceans. J. Geophys. Res. Oceans 123 (11), 7651–7677.

Le Traon, P., Hernandez, F., 1992. Mapping the oceanic mesoscale circulation: Validation of satellite altimetry using surface drifters. J. Atmos. Ocean. Technol. 9 (5), 687–698.

Le Vu, B., Stegner, A., Arsouze, T., 2018. Angular Momentum Eddy Detection and tracking Algorithm (AMEDA) and its application to coastal eddy formation. J. Atmos. Ocean. Technol. 35 (4), 739–762.

Lehahn, Y., d'Ovidio, F., Lévy, M., Heifetz, E., 2007. Stirring of the northeast Atlantic spring bloom: A Lagrangian analysis based on multisatellite data. J. Geophys. Res. 112 (C8), C08005. http://dx.doi.org/10.1029/2006JC003927, URL: http://doi.wiley.com/10.1029/2006JC003927.

Levy, M., Martin, A.P., 2013. The influence of mesoscale and submesoscale heterogeneity on ocean biogeochemical reactions: Influence of heterogeneity. Glob. Biogeochem. Cycles 27 (4), 1139–1150. http://dx.doi.org/10.1002/2012GB004518, URL: http://doi.wiley.com/10.1002/2012GB004518.

Maximenko, N., Niiler, P., Centurioni, L., Rio, M.-H., Melnichenko, O., Chambers, D., Zlotnicki, V., Galperin, B., 2009. Mean dynamic topography of theRapp. Comm. Int. Mer. Medit., 38 pp., 2007. ocean derived from satellite and drifting buoy data using three different techniques. J. Atmos. Ocean. Technol. 26 (9), 1910–1919.

McGillicuddy Jr, D.J., 2016. Mechanisms of physical-biological-biogeochemical interaction at the oceanic mesoscale. Annu. Rev. Mar. Sci. 8, 125–159.

Mead, J., 2005. Assimilation of simulated float data in Lagrangian coordinates. Ocean Model. 8 (4), 369–394.

Menna, M., Poulain, P.-M., Bussani, A., Gerin, R., 2018. Detecting the drogue presence of SVP drifters from wind slippage in the Mediterranean Sea. Measurement 125, 447–453.

Menna, M., Poulain, P.-M., Zodiatis, G., Gertman, I., 2012. On the surface circulation of the levantine sub-basin derived from Lagrangian drifters and satellite altimetry data. Deep Sea Res. I 65, 46–58.

Millot, C., Taupier-Letage, I., 2005. Circulation in the Mediterranean Sea. In: Saliot, A. (Ed.), The Mediterranean Sea, Vol. 5K. Springer Berlin Heidelberg, Berlin, Heidelberg, pp. 29–66. http://dx.doi.org/10.1007/b107143, URL: http://link.springer.com/10.1007/b107143.

Mkhinini, N., Coimbra, A.L.S., Stegner, A., Arsouze, T., Taupier-Letage, I., Béranger, K., 2014. Long-lived mesoscale eddies in the eastern Mediterranean Sea: Analysis of 20 years of AVISO geostrophic velocities. J. Geophys. Res. Oceans 119 (12), 8603–8626.

Muscarella, P., Carrier, M.J., Ngodock, H., Smith, S., Lipphardt Jr, B., Kirwan Jr, A., Huntley, H.S., 2015. Do assimilated drifter velocities improve Lagrangian predictability in an operational ocean model? Mon. Weather Rev. 143 (5), 1822–1832.

Niiler, P.P., 2003. Near-surface dynamical structure of the Kuroshio Extension. J. Geophys. Res. 108 (C6), 3193. http://dx.doi.org/10.1029/2002JC001461, URL: http://doi.wiley.com/10.1029/2002JC001461.

Nodet, M., 2006. Variational assimilation of Lagrangian data in oceanography. Inverse Problems 22 (1), 245.

Pessini, F., Cotroneo, Y., Olita, A., Sorgente, R., Ribotti, A., Jendersie, S., Perilli, A., 2020. Life history of an anticyclonic eddy in the Algerian basin from altimetry data, tracking algorithm and in situ observations. J. Mar. Syst. 207, 103346. http://dx.doi.org/10.1016/j.jmarsys.2020.103346, URL: https://linkinghub.elsevier.com/retrieve/pii/S0924796320300427.

Poulain, P.-M., Bussani, A., Gerin, R., Jungwirth, R., Mauri, E., Menna, M., Notarstefano, G., 2013. Mediterranean surface currents measured with drifters: From basin to subinertial scales. Oceanography 26 (1), 38–47.

Poulain, P.-M., Gerin, R., Mauri, E., Pennel, R., 2009. Wind effects on drogued and undrogued drifters in the eastern Mediterranean. J. Atmos. Ocean. Technol. 26 (6), 1144–1156.

Poulain, P.-M., Menna, M., Mauri, E., 2012. Surface geostrophic circulation of the Mediterranean Sea derived from drifter and satellite altimeter data. J. Phys. Oceanogr. 42 (6), 973–990.

Puillat, I., Taupier-Letage, I., Millot, C., 2002. Algerian eddies lifetime can near 3 years. J. Mar. Syst. 31 (4), 245–259.

Pujol, M.-I., Larnicol, G., 2005. Mediterranean sea eddy kinetic energy variability from 11 years of altimetric data. J. Mar. Syst. 58 (3–4), 121–142.

Rio, M.H., Pascual, A., Poulain, P.-M., Menna, M., Barceló-Llull, B., Tintoré, J., 2014. Computation of a new mean dynamic topography for the Mediterranean Sea from model outputs, altimeter measurements and oceanographic in situ data. Ocean Sci. 10 (4), 731–744.

Robinson, A.R., Leslie, W.G., Theocharis, A., Lascaratos, A., 2001. Mediterranean sea circulation. Ocean Curr. 1, 19.

Robinson, A.R., Malanotte-Rizzoli, P., Hecht, A., Michelato, A., Roether, W., Theocharis, A., Ünlüata, U., Pinardi, N., Artegiani, A., Bergamasco, A., et al., 1992. General circulation of the Eastern Mediterranean. Earth-Sci. Rev. 32 (4), 285–309.

Sarangi, R.K., 2012. Observation of oceanic eddy in the northeastern arabian sea using multisensor remote sensing data. Int. J. Oceanogr. 2012, 1–9. http://dx.doi.org/10.1155/2012/531982, URL: https://www.hindawi.com/journals/ijocean/2012/531982/.

Schroeder, K., Garcìa-Lafuente, J., Josey, S.A., Artale, V., Nardelli, B.B., Carrillo, A., Gacic, M., Gasparini, G.P., Herrmann, M., Lionello, P., et al., 2012. Circulation of the Mediterranean Sea and its variability. In: Lionello, P. (Ed.), The Climate of the Mediterranean Region. Elsevier, pp. 187–256.

Stanichny, S.V., Kubryakov, A.A., Soloviev, D.M., 2016. Parameterization of surface wind-driven currents in the Black Sea using drifters, wind, and altimetry data. Ocean Dyn. 66 (1), 1–10.

Sutyrin, G., Stegner, A., Taupier-Letage, I., Teinturier, S., 2009. Amplification of a surface-intensified eddy drift along a steep shelf in the Eastern Mediterranean Sea. J. Phys. Oceanogr. 39 (7), 1729–1741.

Taillandier, V., Griffa, A., Poulain, P.-M., Béranger, K., 2006. Assimilation of Argo float positions in the north western Mediterranean Sea and impact on ocean circulation simulations. Geophys. Res. Lett. 33 (11), L11604. http://dx.doi.org/10.1029/2005GL025552.

Talagrand, O., Courtier, P., 1987. Variational assimilation of meteorological observations with the adjoint vorticity equation. I: Theory. Q. J. R. Meteorol. Soc. 113 (478), 1311–1328.

Taupier-Letage, I., Barbanti, R., El Gindy, A., Emelianov, M., Fuda, J.-L., Font, J., Gerin, R., Guillerm, C., Julia, A., Mauri, E., Millot, C., Poulain, P.-M., Notarstefano, G., Rougier, G., Said, M., 2007. New Elements on the Surface Circulation in the Eastern Basin of the Mediterranean, Vol. 38. Technical Report, CIESM 38th Congress, Rapp. Comm. Int. Mer Medit., Istanbul, Turkey, p. 204, April 2007.

Taupier-Letage, I., Puillat, I., Raimbault, P., Millot, C., 2003. Biological response to mesoscale eddies in the Algerian Basin. J. Geophys. Res. 108 (C8), 3245–3267. http://dx.doi.org/10.1029/1999JC000117, URL: http://doi.wiley.com/10.1029/1999JC000117.

Testor, P., de Young, B., Rudnick, D.L., Glenn, S., Hayes, D., Lee, C.M., Pattiaratchi, C., Hill, K., Heslop, E., Turpin, V., et al., 2019. Oceangliders: a component of the integrated GOOS. Front. Mar. Sci. 6, 422.

Tonani, M., Pinardi, N., Dobricic, S., Pujol, I., Fratianni, C., 2008. A high-resolution free-surface model of the Mediterranean Sea. Ocean Sci. Eur. Geosci. Union 4 (1), 1–14.

Uchida, H., Imawaki, S., 2003. Eulerian mean surface velocity field derived by combining drifter and satellite altimeter data: Eulerian mean surface velocity field. Geophys. Res. Lett. 30 (5), 1229. http://dx.doi.org/10.1029/2002GL016445, URL: http://doi.wiley.com/10.1029/2002GL016445.

Weaver, A., Courtier, P., 2001. Correlation modelling on the sphere using a generalized diffusion equation. Q. J. R. Meteorol. Soc. 127 (575), 1815–1846.